Self-similar transport of inertial particles in a turbulent boundary layer

G. Sardina, P. Schlatter, F. Picano, C. M. Casciola, L. Brandt and D. S. Henningson

Journal of Fluid Mechanics / Volume 706 / September 2012, pp 584 - 596
DOI: 10.1017/jfm.2012.290, Published online: 13 July 2012

J. Fluid Mech. (2012), *vol.* 706, *pp.* 584–596.
doi:10.1017/jfm.2012.290

Self-similar transport of inertial particles in a turbulent boundary layer

G. Sardina[1,3]†, P. Schlatter[1], F. Picano[1,2], C. M. Casciola[2], L. Brandt[1] and D. S. Henningson[1]

[1] Linné FLOW Centre and SeRC (Swedish e-Science Research Centre), KTH Mechanics, SE-100 44 Stockholm, Sweden

[2] Dipartimento di Ingegneria Meccanica e Aerospaziale, Sapienza University of Rome, 00184 Rome, Italy

[3] Facoltà di Ingegneria, Architettura e Scienze Motorie, UKE–Università Kore di Enna, 94100 Enna, Italy

(Received 28 March 2012; revised 13 May 2012; accepted 12 June 2012; first published online 13 July 2012)

Results are presented from a direct numerical simulation of a particle-laden spatially developing turbulent boundary layer up to $Re_\theta = 2500$. The peculiar feature of a boundary-layer flow seeded with heavy particles is the variation of the local dimensionless parameters defining the fluid–particle interactions along the streamwise direction. Two different Stokes numbers can be defined, one using inner flow units and the other with outer units. Since these two Stokes numbers exhibit different decay rates in the streamwise direction, we find a decoupled particle dynamics between the inner and the outer region of the boundary layer. Preferential near-wall particle accumulation is similar to that observed in turbulent channel flow, while different behaviour characterizes the outer region. Here the concentration and the streamwise velocity profiles are found to be self-similar and to depend only on the local value of the outer Stokes number and the rescaled wall-normal distance. These new results are powerful in view of engineering and environmental applications and corresponding flow modelling.

Key words: boundary layers, multiphase and particle-laden flows, turbulent flows

1. Introduction

The dispersion of inertial particles in turbulent boundary layers is relevant to many engineering and environmental applications. For instance, interactions between volcanic ash and aeroplanes are one possible origin of several failures in aeronautical engines. In this case, the turbine blades can be seriously damaged by the small and heavy particles dispersed inside the volcanic ash clouds (Grindle, Burcham & Hugh 2003). From an environmental point of view, the dispersion of pollutants in the atmospheric boundary layer or along rivers, for example, are typical examples of interactions between particles and wall-bounded turbulent flows. As an additional example, Chamecki & Meneveau (2011) recently proposed theoretical predictions of a particle-laden turbulent boundary layer to model pollen dispersion on crop fields. Their analytical results have been also validated by large eddy simulations. The prediction of pollen dynamics in the atmosphere assumes a crucial role in investigation of

† Email address for correspondence: gaetano@mech.kth.se

genetic diversity in populations (O'Connell, Mosseler & Rajora 2007) and ecological risks derived by the use of genetically modified crops (Messeguer 2003). The pollen density ratio (with respect to air) is of the order of one thousand, and the diameter order of 10–100 μm, thus sufficiently smaller than the smallest characteristic scale of the flow, the so-called Kolmogorov scale. Similarly, the related relaxation times are $\tau_p \equiv \rho_p d_p^2/18\rho_f \nu = 0.15$–$46$ ms (Chamecki & Meneveau 2011), where ρ_p is the particle density, d_p is the particle diameter, and ρ_f and ν are the fluid density and kinematic viscosity.

The main parameter that controls the dynamics of particles in turbulent flow is the so-called Stokes number, St, which is the ratio between the particle relaxation time and a characteristic time scale of the flow: see e.g. Toschi & Bodenschatz (2009) and Balachandar & Eaton (2010) for recent reviews. The characteristic phenomenon of wall-bounded flow is turbophoresis: preferential particle accumulation at the wall. The term turbophoresis literally means transport operated by turbulence, and it appeared for the first time in the literature in the theoretical work by Caporaloni *et al.* (1975). In the last twenty years a large number of experiments and numerical simulations have been performed to study wall particle accumulation. Kaftori, Hetsroni & Banerjee (1995*a*,*b*) investigated particle dynamics close to the wall by means of visualization techniques and laser Doppler anemometry (LDA) measurements in a water flume. They focused their efforts on the role of the coherent structures in particle motion and particle deposition in the wall layer. Righetti & Romano (2004) showed the modifications of the mean streamwise velocity and Reynolds stress in a open channel flow seeded with particles. More recently, Gerashchenko *et al.* (2008) performed experiments in a boundary layer focusing on inertial particle accelerations in the wall region. In particular, they observed an increase in the acceleration variance by increasing the Stokes number, exactly the opposite to that observed in homogeneous isotropic turbulence (Bec *et al.* 2006). Besides experimental work, many direct numerical simulations can be found in the literature. Rouson & Eaton (2001) noted a strong correlation between sweep-ejection events and wall particle deposition by looking at the results of direct numerical simulation of a channel flow. Marchioli & Soldati (2002) examined the modification of particle velocity statistics due to the presence of coherent structures in the buffer layer. Recently, the large-scale simulation by Sardina *et al.* (2011) showed that the artificial periodicity in the streamwise and spanwise directions imposed in numerical simulations may alter the particle distribution at the wall with differences of up to ten per cent.

Parallel flows such as channels, open channels and pipes are typically employed in both simulations and experiments. These are statistically homogeneous in the flow direction, and the particle Stokes number does not change during the time evolution. In addition, the particle motion is typically assumed periodic along the channel/pipe length and so only the statistical steady state is analysed. Spatially evolving simulations can be useful in order to characterize typical lengths needed to achieve a statistical steady state and to investigate the transient phase: see Picano, Sardina & Casciola (2009). A spatially changing local Stokes number can bring anomalous phenomena into the transport as observed in particle-laden jet flows (Picano *et al.* 2010), where an unexpected preferential particle accumulation is found near the jet axis when the local Stokes number is of order unity.

In this context, the study of particle dynamics in spatially evolving boundary layers may help in advancing our understanding of multiphase flows because it combines these two effects: (i) Stokes number variation in the main stream direction, and (ii) spatially evolving flow configuration. We address here particle dynamics in a

boundary layer with zero-pressure gradient up to Reynolds number $Re_\theta = 2500$, based on the momentum-loss thickness θ and free-stream velocity U_∞, in a large computational domain to avoid incorrect estimation of wall particle concentrations (Sardina *et al.* 2011, 2012). The corresponding friction Reynolds number towards the end of the domain is $Re_\tau = 800$, based on the local friction velocity $U_\tau \equiv \sqrt{\tau_w/\rho}$ (where τ_w is the local wall-shear stress) and 99 % boundary-layer thickness δ_{99}. This is the first simulation of a particle-laden turbulent boundary layer we are aware of, presumably with the highest Reynolds number for inertial particle dynamics in wall flows. The pollen dispersion simulations described in Chamecki & Meneveau (2011) are large eddy simulations with low inertia particles modelled in an Eulerian framework. We recall that in the closely related field of bubble-laden flows, Ferrante & Elghobashi (2007) studied the effects of micro-bubbles in a turbulent boundary layer up to $Re_\theta = 2900$ and, more recently, Mattson & Mahesh (2011) performed a one-way coupling simulation for bubble dynamics in turbulent boundary layers up to $Re_\theta = 1800$.

For inertial particles, a nominal Stokes number St_0 can be defined by using the constant free-stream velocity U_∞ and the displacement thickness of the boundary layer at the inflow δ_0^*, $St_0 \equiv \tau_p U_\infty/\delta_0^*$. This global parameter quantifies the inertia of a single population of monodisperse particles. For a spatially evolving flow, local Stokes numbers should be defined in terms of local variables. In turbulent boundary layers two different scalings are traditionally used: the so-called inner scaling in terms of wall units $y^+(x) \equiv y/(\nu/U_\tau(x))$, and an outer scaling $y/\delta^*(x)$ where δ^* is the local displacement thickness of the boundary layer. Two Stokes numbers are therefore defined: St^+ in local inner units and St_{δ^*} in outer units,

$$St^+ \equiv \frac{\tau_p U_\tau^2}{\nu}, \quad St_{\delta^*} \equiv \frac{\tau_p U_\infty}{\delta^*}. \tag{1.1}$$

Since U_τ diminishes while δ^* increases, the two Stokes numbers vanish sufficiently far downstream and particles eventually behave as passive tracers. In the presence of gravity, the particle dynamics is controlled by a second non-dimensional number, the Froude number, and the particle dynamical equation, scaled with outer acceleration U_∞^2/δ^* (prime $'$ denotes non-dimensional quantities), reads (Maxey & Riley 1983):

$$\frac{\mathrm{d}v'}{\mathrm{d}t'} = \frac{u' - v'}{St_{\delta^*}} + g\frac{\delta^*}{U_\infty^2}, \tag{1.2}$$

where g is the gravitational acceleration, and u and v are the fluid and particle velocity, respectively. In the limit of large Stokes number St_{δ^*}, the non-dimensional velocity difference is finite, so that $|u - v| \propto u'_{rms} \propto U_\infty$. In these conditions, the Stokes drag is the leading term when $1/St_{\delta^*} \gg g\delta^*/U_\infty^2$, or equivalently

$$U_\infty \gg \tau_p g \equiv u_g, \tag{1.3}$$

where u_g is the settling velocity. Hence gravity is negligible when the particle Froude number $Fr_p \equiv U_\infty/(\tau_p g) \gg 1$. Considering the example of pollen discussed in the Introduction where the particle relaxation time is $\tau_p \simeq 10^{-4}$–10^{-1} s, gravity becomes negligible for a streamwise velocity $U_\infty \simeq 10$ m s^{-1} or larger.

In the limit of small Stokes numbers $St_{\delta^*} \ll 1$, it is well established (Bec *et al.* 2006; Picano *et al.* 2011) that the particle acceleration can be correctly approximated

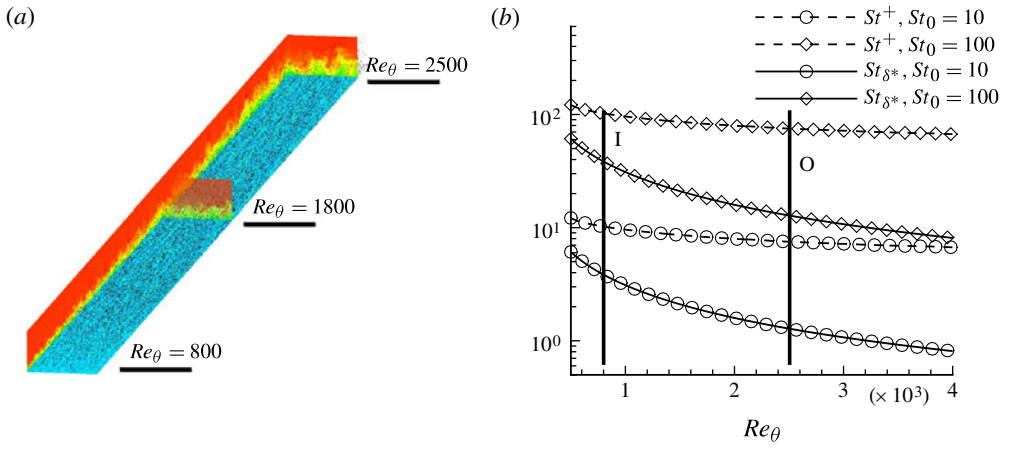

FIGURE 1. (*a*) Instantaneous configuration of inertial particles with $St^0 = 30$ inside our computational domain. (*b*) Development of the local inner (St^+) and outer (St_{δ^*}) Stokes number in the streamwise direction for two fixed particle populations characterized by a nominal Stokes number of 10 and 100. The letters I and O indicate the streamwise position of the injection point and the end of the domain for the present simulation.

by the fluid acceleration and

$$a_p' \simeq a_f' = \frac{u' - v'}{St_{\delta^*}} + g\frac{\delta^*}{U_\infty^2}. \tag{1.4}$$

Hence, given the fluid acceleration, the particle velocity can be expressed as

$$v' = u' - St_{\delta^*}\left(a_f' + g\frac{\delta^*}{U_\infty^2}\right). \tag{1.5}$$

From the above, we see that in the limit of vanishing Stokes number, $St_{\delta^*} \to 0$, the particle velocity perfectly matches that of the fluid and particles behave as passive tracers. If the Stokes number is small, though finite, the fluid acceleration a_f scales with U_∞^2/δ^* in the outer region, so $a_f' = a_f\,\delta^*/U_\infty^2 = O(1)$ and for gravity to be negligible

$$g\frac{\delta^*}{U_\infty^2} \ll 1. \tag{1.6}$$

This is equivalent to $Fr \equiv U_\infty/\sqrt{g\delta^*} \gg 1$, with Fr the flow Froude number. Since the thickness δ^* increases downstream, eventually gravity becomes relevant. Note however that for $U_\infty \simeq 10$ m s^{-1}, δ^* should be of the order of 10 m, which corresponds to a very large Reynolds number, i.e. $Re_\theta \simeq 10^7$.

A sketch of the geometric configuration is shown in figure 1(*a*), where an instantaneous flow field is plotted together with particle positions, indicated with dots, for the case $St_0 = 30$. In figure 1(*b*) the behaviour of the two local Stokes number is shown versus Re_θ for two particle populations $St_0 = 10, 100$. Data are taken from the simulations of single-phase fluid by Schlatter & Örlü (2010). It is interesting to note that the Stokes number based on the outer scale decays faster. The location where particles are injected in the simulation is indicated by I, particle inlet section, whereas O denotes the end of the computational domain.

2. Numerical methodology

A direct numerical simulation (DNS) of a particle-laden turbulent boundary layer was performed by means of the pseudo-spectral code SIMSON developed at KTH during the last twenty years (Chevalier *et al.* 2007). One-way coupling is assumed to model particle–flow interactions. In this context, data from unladen simulations for the flow are already available based on previous experience at KTH in this field: see Schlatter *et al.* (2009) and Schlatter & Örlü (2010). The present computational domain is $x_L \times y_L \times z_L = 3000\delta_0^* \times 100\delta_0^* \times 120\delta_0^*$ in the streamwise, wall-normal and spanwise directions based on the displacement thickness δ_0^* at the (laminar) domain inlet characterized by $Re_{\delta 0}^* \equiv U_\infty \delta_0^*/\nu = 450$. The resolution involves $n_x \times n_y \times n_z = 4096 \times 301 \times 384$ spectral modes, where n_x and n_z are the number of Fourier modes in the streamwise and spanwise directions and n_y is the number of Chebyshev modes in the wall-normal direction. Because the boundary-layer flow is spatially evolving, a fringe region technique at the end of the computational domain is used to ensure that the flow is forced back to the laminar inflow profile at the inlet. Geometry and flow parameters are essentially the same as in the simulation described in Schlatter *et al.* (2009). In order to reach a fully developed turbulent flow, the carrier phase needs to reach a Reynolds number $Re_\theta \simeq 1600$. In the present case, Re_θ at the end of the domain is 2500. In addition, it is important to start with a relatively low Reynolds number at the inflow $Re_\theta \simeq 200$ and trip the flow to turbulence via a localized forcing random in both time and the spanwise direction. For more details on the fluid phase, the reader is referred to Schlatter *et al.* (2009).

Concerning the dispersed phase, one-way coupling was assumed to model particle–flow interactions, based on the assumption that the particles were very diluted. The particles were assumed to be smaller than the Kolmogorov scale (sub-Kolmogorov), i.e. rigid spheres with density of order one thousand times the density of the carrier phase. Gravity was neglected, as justified above, and the particles were subjected only to Stokes drag (Maxey & Riley 1983). The pseudo-spectral code coupled with a Lagrangian solver was validated for channel flow simulation in very large domains: see Sardina *et al.* (2011, 2012). For the present case we improved the order of interpolation of the fluid velocity at particle position from second to fourth order, using Hermite interpolation in the wall-normal direction and fourth-order standard interpolation in the streamwise/spanwise directions, whilst time integration for particle trajectories was performed using second-order Adams–Bashforth. Eight different populations, each characterized by a specific nominal Stokes number St_0, were examined. Particles were injected at a constant rate into the already turbulent flow at $Re_\theta \simeq 800$ so that they were not directly influenced by the trip forcing and the resulting transitional flow. They were introduced randomly in the spanwise direction at several fixed and equispaced wall-normal positions between the wall and the local coordinate $4\delta_{99}$; initially the particle velocity was equal to the local flow velocity. In this way, many of the particles were initially injected outside the boundary layer in the laminar free stream. The particle concentration at the wall reached quasi-steady state after $\sim 70\,000\delta_0^*/U_\infty$ time units. After that we collected statistics for another $10\,000\delta_0^*/U_\infty$ units. The simulation was run on 1536 cores on a Cray XE6 system using a hybrid MPI/OpenMP parallelization, recently developed to improve the performance of the Eulerian–Lagrangian coupled spectral solver SIMSON.

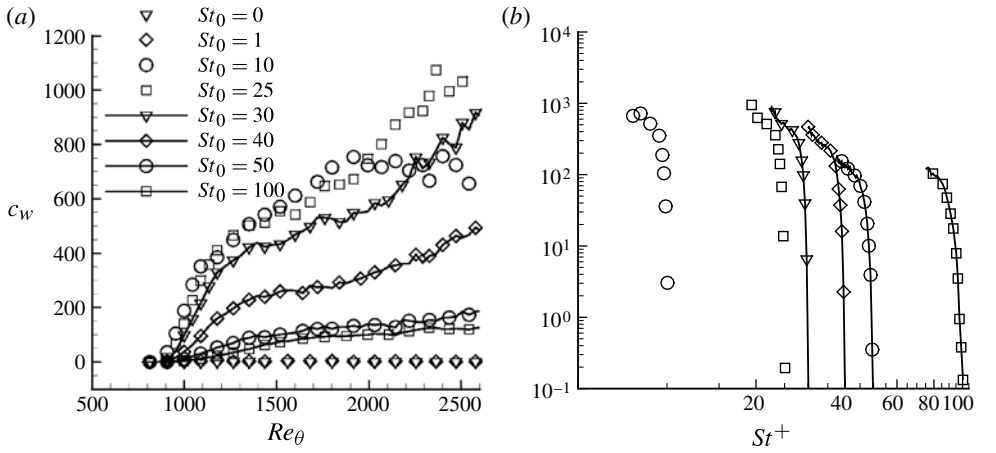

FIGURE 2. (*a*) Particle concentration close to the wall versus the streamwise coordinate, represented by Re_θ. (*b*) Particle wall concentration plotted against the local viscous Stokes number St^+.

3. Results

The particle concentration at the wall is plotted against the streamwise position identified by Re_θ for the different populations considered in figure 2(*a*). The wall concentration is defined as the number of particles per unit volume that each particle population assumes below a given distance from the wall (here $0.01\delta_0^*$).

The first phase of the accumulation process is characterized by a strong particle drift towards the wall. This drift is quantified by the local slope of the concentration profiles. Particles introduced at $Re_\theta \simeq 800$ are subject to an intense turbophoretic process starting at $Re_\theta = 900$. The distance over which this phase is completed depends on the particle inertia, typically $Re_\theta = 1100$–1500. The particle populations characterized by a nominal Stokes number of 10 and 25 initially exhibit the highest accumulation growth. This first transient is followed by a secondary growth characterized by a lower slope. All the populations with St_0 greater than 10 remain in this second accumulation phase until the end of the computational domain; the particles characterized by $St_0 = 25, 30$ assume the highest values of wall concentration.

A peak in the streamwise distribution of wall concentration is reached only by particles with $St_0 = 10$ within the computational domain, namely at $Re_\theta \simeq 2200$. Downstream of the peak, we see a slight decrease in the concentration at the wall, indicating a slow approach to the tracer limit. Capturing the concentration peak for the heaviest population would have required a longer computational domain. Indeed, theoretically, in an infinitely long domain all the particle populations will reach a concentration peak after the second, slower, accumulation phase, with the peak position obviously a function of the particle inertia. Downstream of the location of maximum accumulation, the concentration at the wall will diminish as the particles tend to the Lagrangian limit, i.e. the viscous Stokes number decreases. However, the viscous Stokes number is proportional to the friction coefficient c_f and thus approximately proportional to $Re_\theta^{-1/4}$ in a turbulent boundary layer. In other words, particles of nominal Stokes number 10 reach a local viscous Stokes number of order one only at Re_θ larger than 10^7, beyond the reach of present-day simulations or well-controlled laboratory experiments.

The wall concentration is plotted as a function of the local viscous Stokes number in figure 2(*b*). This plot shows the differences between the boundary layer and the channel flow: in the boundary layer an equilibrium wall concentration is never reached except for the trivial case of pure Lagrangian tracers, whereas in channels the viscous Stokes number St^+ remains constant and a fully developed state is observed.

It is known from channel flow simulations (Marchioli & Soldati 2002) that the particles most subject to turbophoresis are characterized by a viscous Stokes number of order $St^+ \approx 20, 25$ and therefore we report in figure 2(*b*) the wall concentration as a function of the local viscous Stokes number. Here, it is interesting to note that in homogeneous isotropic turbulence the maximum clustering occurs when the Stokes number based on the characteristic scale of the smallest vortices, the Kolmogorov time, is of order one. In wall-bounded flows, the maximum turbophoresis occurs when the Stokes number based on the time scale of the vortical structures in the buffer layer is order one, which corresponds to a viscous Stokes number $\sim$25 at moderate Reynolds numbers. Usually, the two phenomenologies of clustering and turbophoresis have been described separately. Nevertheless they are not distinct and they are clearly linked, as shown in Sardina *et al.* (2012); in particular, turbophoresis cannot exist if there is no clustering of inertial particles in the buffer layer. Note that for every population St^+ diminishes by 25 % in the streamwise direction between the injection point and the end of the domain. For the maximally accumulating particles, $St_0 = 25$–30, the largest concentration values are found for $St^+ = 20$ and 22 respectively. These values are close to those found in channel flows, which suggests that turbophoresis is essentially dominated by the near-wall dynamics. It is important to stress that for particle populations in the range $St_0 = 25$–50, the concentration at the wall seems to depend only on the local Stokes number after a small initial transient. Memory effects, due to the combination of initial conditions and inertial particle dynamics, may explain the difference in accumulation observed for different populations at the same local Stokes number. The reader is also referred to Picano *et al.* (2010), where similar effects have been observed in spatially developing particle-laden jets.

By looking at the wall-normal concentration profile in the outer region of the boundary layer, another difference between particle-laden channel flow and particle-laden boundary layers emerges clearly. Whereas in the channel flow the concentration profile is monotonically decreasing from the wall towards the channel centre, in the boundary layer the concentration profile of particles with finite inertia is characterized by a local minimum at a distance from the wall approximately corresponding to the local displacement thickness of the boundary layer, δ^*. Turbophoresis is associated with a net flux of particles from the bulk flow towards the wall and, in channel flows, due to the wall-normal symmetry, the zone eventually most depleted of particles is around the centreline. In spatially developing turbulent boundary layers, however, the particle concentration is fixed in the free stream to the initial undisturbed value. Hence, the depletion of particles in the shear layer, combined with the fixed concentration in the free stream, creates the observed minimum, occurring at $\delta^* \simeq 1$. We report in figure 3(*a*) the wall-normal concentration profile at $Re_\theta = 2500$ for three different populations. The concentration is normalized with its minimum value c_{min} and the wall-normal coordinate with the local displacement thickness δ^*. As stated before, this minimum value occurs around a wall-normal distance of one displacement thickness; further away from the wall the particle concentration is monotonically increasing. In addition, one can see that the heaviest particles, $St_0 = 100$, exhibit a local maximum at the boundary-layer edge, i.e. at the geometric thickness of the boundary layer $\delta_{99} \simeq 5.5\delta^*$ at $Re_\theta = 2500$; this unexpected behaviour is absent in channel flows.

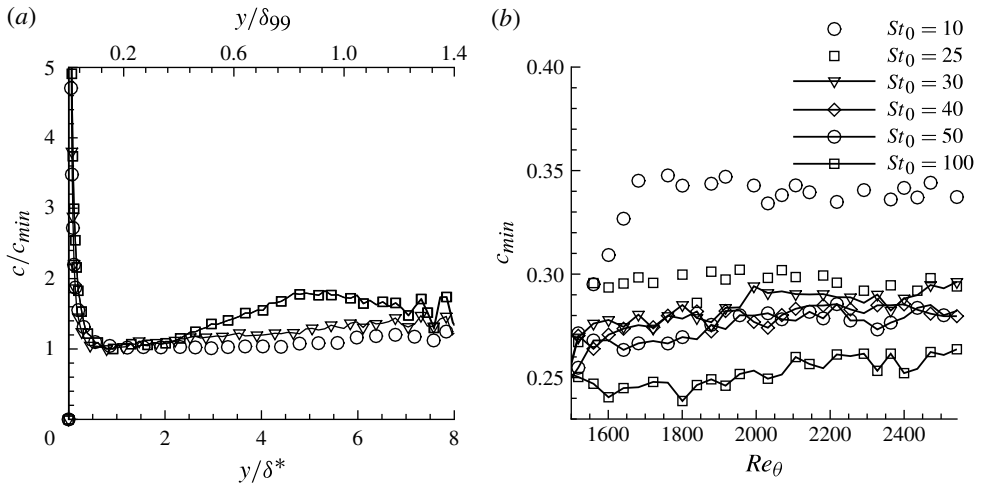

FIGURE 3. (*a*) Normalized wall-normal particle concentration for the three populations indicated in the legend at $Re_\theta = 2500$. (*b*) Minimum particle concentration versus the streamwise direction for the different populations.

To provide additional details of the particle concentration profile in the outer region, we show the evolution of the concentration minimum in the streamwise direction for the different nominal Stokes numbers St_0 in figure 3(*b*). The minimum appears during the second, slower accumulation phase described above, downstream of $Re_\theta = 1500$ in our configuration. The value of c_{min} does not change significantly with Re_θ; in particular, the particles with $St_0 = 10$ show a slight decrease whereas heavier populations tend to continuously increase the value of the concentration in the mean flow direction. Furthermore, we note that the value of the minimum concentration decreases with particle inertia.

One of the main findings of the present work is that, by properly normalizing the DNS data, a self-similar solution for the concentration profile in outer variables clearly emerges, as demonstrated in figure 4. This self-similar behaviour is found after $Re_\theta = 1500$, therefore during the second part of the accumulation process, after the appearance of the concentration minimum at $y \approx \delta^*$ discussed above.

According to our results, the outer concentration profile can be written as

$$\frac{c(x, y, \tau_p, U_\infty, \nu)}{c_{min}(x, \tau_p, U_\infty, \nu)} \equiv \frac{c\left(Re_\theta, \dfrac{y}{\delta^*}, St_0\right)}{c_{min}(Re_\theta, St_0)} \equiv f\left(\frac{y}{\delta^*}, St_{\delta^*}\right). \tag{3.1}$$

In other words, if we divide the wall-normal coordinate by the local displacement thickness $\delta^*(x)$, and divide the concentration by its minimum value, c_{min}, concentration profiles pertaining to different particle populations collapse onto a unique curve parametrized by the local value of the Stokes number St_{δ^*}. In figures 4(*a*) and 4(*b*) we plot the concentration profiles of different particle populations, $St_0 = 25, 30, 40$ and $St_0 = 30, 40, 50$, respectively, extracted at different streamwise distances, $Re_\theta = 1600, 1900, 2500$ and $Re_\theta = 1500, 2000, 2500$, while keeping constant the local Stokes number based on the displacement thickness, $St_{\delta^*} = 5$ and $St_{\delta^*} = 6.4$. It should be noted that the self-similarity of the outer concentration implies that the profiles given

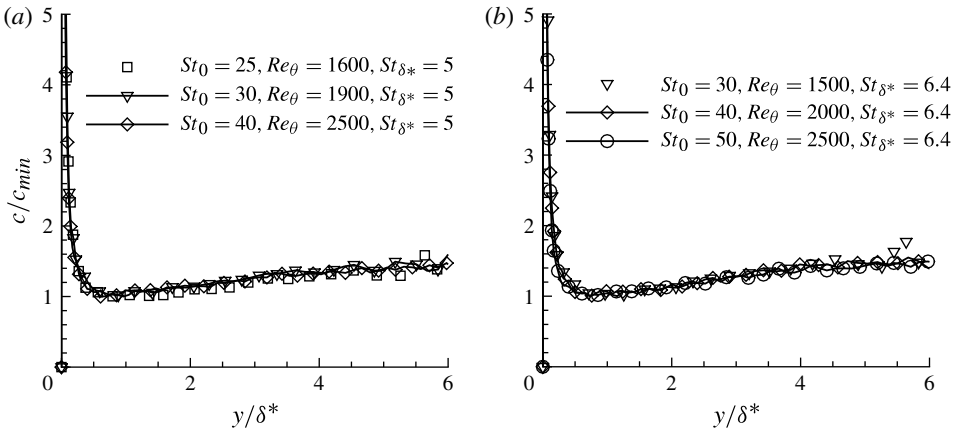

FIGURE 4. Wall-normal particle concentration profile for three populations characterized by the same local Stokes number based on the displacement thickness. (*a*) $St^*_\delta = 5$ and (*b*) $St^*_\delta = 6.4$, taken from different populations at different streamwise positions.

by (3.1) cannot depend on Re_θ since we are dealing with different inertia (i.e. St_0) and different streamwise positions (i.e. Re_θ), but the same St^*_δ.

We stress that the two profiles in figure 4(*a*,*b*) do not differ in a clear way simply because the range of variation of the local Stokes number $St_{\delta*}$ is small in this case. We expect the concentration profile to depend on the Stokes number; further downstream, for vanishing Stokes numbers, the Lagrangian limit should eventually be recovered and the profile should become uniform. Moreover, at $St_{\delta*} \approx 10$ a second peak in the concentration profile appears around the geometric thickness of the boundary layer δ_{99}, as shown in figure 3(*a*) for the population with $St_0 = 100$. Although the limited number of populations evolved in the simulation and the restrictions imposed on the streamwise length of the domain, both limited by computational resources, do not allow us to explore the self-similar behaviour of particle concentrations over a larger range of local Stokes numbers $St_{\delta*}$, the trend is clear.

The existence of a self-similar solution for the wall-normal concentration profile is suggested by the theoretical work in Chamecki & Meneveau (2011) for the case of pollen (relatively low Stokes numbers). In that case, the particles are mostly subject to gravity while the Stokes drag is negligible. They are continuously injected in the domain from the wall at a constant rate and a complete self-similar solution is found, from the inner to the outer wall region. In our case, the inertial particles are injected across the shear layer, and the inner-layer self-similarity is not fulfilled since the wall accumulation is not constant in the mean flow direction but varies with the local viscous Stokes number. At the same time, the outer layer is governed by the outer Stokes number, which decays downstream at a different rate than the viscous Stokes number, as shown in figure 1(*b*).

In figure 5(*a*) we show that not only the concentration but also the particle streamwise velocity of different populations of the same outer Stokes number $St_{\delta*}$ collapse in a unique profile when rescaling the wall-normal coordinate with the local displacement thickness. Hence the streamwise particle velocity also has self-similar behaviour in the outer region, and the particle dynamics is governed only by the local Stokes number. It is well accepted that the streamwise flow velocity is also

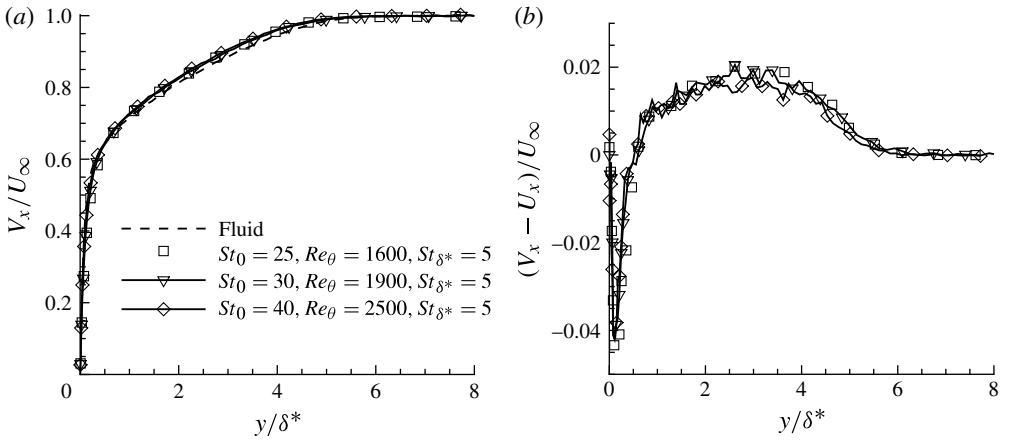

FIGURE 5. (*a*) Streamwise particle velocity profiles for three populations characterized by the same outer local Stokes number St_{δ^*}. (*b*) Profiles of the difference between the average streamwise particle velocity and the average streamwise fluid velocity characterized by the same outer local Stokes number St_{δ^*}.

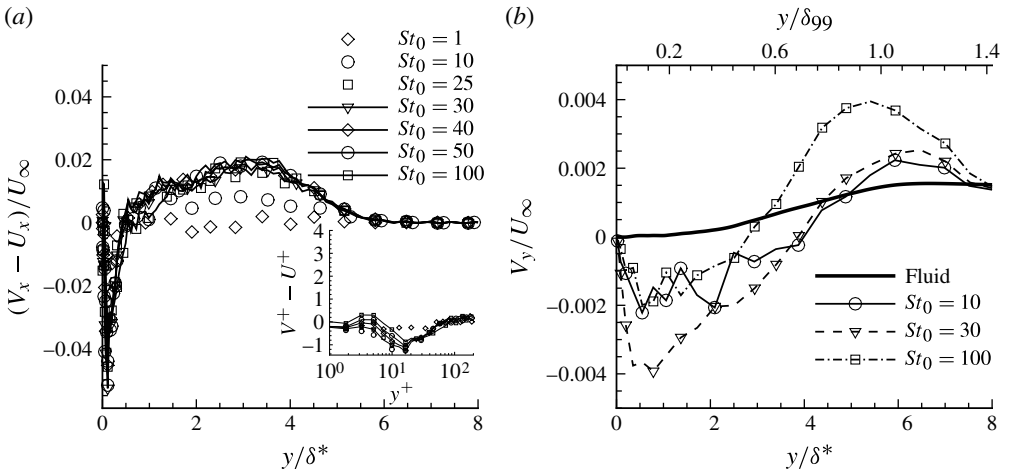

FIGURE 6. (*a*) Wall-normal profiles of the difference between the average streamwise particle velocity and the average streamwise fluid velocity at $Re_\theta = 2500$. In the inset, the same observable is plotted in wall units to emphasize the behaviour of the near-wall region. (*b*) Profiles of the wall-normal particle velocity at $Re_\theta = 2500$.

self-similar in the outer boundary layer (the dashed line in the figure). Consequently, the difference between the streamwise particle and fluid velocity is self-similar, as shown in figure 5(*b*). The velocity of the particle family characterized by the local Stokes number $St_{\delta^*} = 5$ differs from the fluid velocity profile for $y/\delta^* \approx 2$–4; for lower values of St_{δ^*} the particle velocity profile tends to that of the fluid.

To investigate the relative velocity between fluid and particles, we present in figure 6(*a*) the wall-normal distribution of the difference between the average streamwise particle velocity V_x and the average streamwise fluid velocity U_x. Close

to the wall, particles are slower than the carrier phase. Since in the near-wall region of wall-bounded flows, particles tend to stay preferentially in the slow-speed regions (Marchioli & Soldati 2002; Picano *et al.* 2009), we ascribe this behaviour to the same phenomenology. The behaviour in the near-wall region is emphasized in the inset of figure 6(*a*) where the relative velocity is plotted in wall units. The inertial particles tend to be slower than the carrier phase in the buffer layer while in the viscous region they are again faster than the fluid. In the region between about one displacement thickness δ_* and the layer edge δ_{99}, however, particles are faster than the fluid. This finding is linked to the spatial development of the boundary layer: while the layer is growing in the wall-normal direction, the mean streamwise velocity decreases downstream at the same distance from the wall. Particle inertia partially delays this velocity decay and therefore the solid phase is on average faster than the flow. Close to the boundary-layer thickness δ_{99}, the particle velocity again approaches the fluid velocity. The streamwise velocity profile is almost independent of the Stokes number, except for the lightest particles (nominal Stokes number $St_0 = 1, 10$) that better follow the carrier phase owing to weaker inertial effects. It is interesting to note that in correspondence with the minimum value of the concentration c_{min}, the velocity difference $V_x - U_x$ vanishes, implying a zero average Stokes drag in the streamwise direction. The location $\delta_* \approx 1$ seems to be an equilibrium layer for inertial particles.

Figure 6(*b*) shows the wall-normal particle velocity V_y. Despite the extensive statistics collected, this observable is not yet fully converged. Nevertheless, clear behaviour emerges from the plot, which can explain the observed minimum in the concentration profiles discussed above. In agreement with the minimum wall-normal concentration c_{min} located at $y \simeq \delta_*$, inertial particles drift towards the wall. For $St_0 = 30$, for instance, the maximally wall-accumulating particles, the effect is particularly strong. This behaviour is a characteristic feature of the boundary layer and has no equivalent in the channel flow, where the average wall-normal particle and fluid velocity are identically zero across the channel height. The average wall-normal particle drift in boundary layers is instead systematically directed towards the wall up to $y \simeq 3\delta^*$, implying that turbophoresis is active along the boundary layer, never reaching equilibrium conditions. Interestingly, the mean particle velocity is opposite to the fluid velocity, which in the present boundary layer with zero-pressure gradient is always directed away from the wall. The second (outer) concentration peak, observed in the intermittent region at the boundary-layer edge for $St_0 = 100$, can also be explained in terms of wall-normal particle velocity. As shown in the figure, at the edge of the boundary layer, the heaviest particles ($St_0 = 100$) are the only ones characterized by a strong drift directed away from the wall (about four times the corresponding wall-normal fluid velocity).

4. Conclusions

Self-similar behaviour of the wall-normal particle concentration and streamwise velocity profiles, in the outer region of a spatially developing turbulent boundary layer, is found by means of DNS of particle-laden flow over a flat plate. The particle dynamics in this region is governed only by the local Stokes number based on the boundary-layer displacement thickness. A complete self-similar solution for both inner and outer zone cannot exist, since the near-wall accumulation in the inner region is controlled by the viscous Stokes number, the particle relaxation time divided by the inner time scale of turbulence, and the inner and the outer Stokes numbers decay downstream at different rates. The main analogies and differences between particle-

laden boundary-layer and particle-laden channel flow have been discussed, the former mainly related to the near-wall dynamics. In particular, we note that the different distribution of the wall-normal velocity causes a minimum in the concentration profiles for the boundary-layer case in correspondence to the displacement thickness and, for the heaviest particles, a second maximum concentration at the boundary-layer edge (at around δ_{99}).

Acknowledgements

The authors acknowledge DEISA (Distributed European Infrastructure for Supercomputing Applications) for computer time granted within the project WALLPART. In particular, we thank EPCC (Edinburgh Parallel Computing Centre) for help in setting up the simulation on their computers. Resources at NSC (National Supercomputer Centre) allocated via SNIC (Swedish National Infrastructure for Computing) were used for post-processing the data. We would like to acknowledge the support from COST Action MP0806 'Particles in Turbulence', and discussions with Professors Kuerten and Toschi.

REFERENCES

BALACHANDAR, S. & EATON, J. K. 2010 Turbulent dispersed multiphase flow. *Annu. Rev. Fluid Mech.* **42**, 447–464.

BEC, J., BIFERALE, L., BOFFETTA, G., CELANI, A., CENCINI, M., LANOTTE, A., MUSACCHIO, S. & TOSCHI, F. 2006 Acceleration statistics of heavy particles in turbulence. *J. Fluid Mech.* **550** (1), 349–358.

CAPORALONI, M., TAMPIERI, F., TROMBETTI, F. & VITTORI, O. 1975 Transfer of particles in nonisotropic air turbulence. *J. Atmos. Sci.* **32** (3), 565–568.

CHAMECKI, M. & MENEVEAU, C. 2011 Particle boundary layer above and downstream of an area source: scaling, simulations, and pollen transport. *J. Fluid Mech.* **683** (1), 1–26.

CHEVALIER, M., SCHLATTER, P., LUNDBLADH, A. & HENNINGSON, D. S. 2007 SIMSON: A pseudo-spectral solver for incompressible boundary layer flows. *Tech. Rep.* TRITA-MEK 2007:07, KTH Mechanics.

FERRANTE, A. & ELGHOBASHI, S. E. 2007 Reynolds number effect on drag reduction in a bubble-laden spatially developing turbulent boundary layer. *J. Fluid Mech.* **572**, 145–177.

GERASHCHENKO, S., SHARP, N. S., NEUSCAMMAN, S. & WARHAFT, Z. 2008 Lagrangian measurements of inertial particle accelerations in a turbulent boundary layer. *J. Fluid Mech.* **617** (1), 255–281.

GRINDLE, T. J., BURCHAM, F. W. & HUGH, L. 2003 Engine damage to a NASA DC-8-72 airplane from a high-altitude encounter with a diffuse volcanic ash cloud. NASA/TM-2003-212030.

KAFTORI, D., HETSRONI, G. & BANERJEE, S. 1995*a* Particle behaviour in the turbulent boundary layer. Part 1. Motion, deposition, and entrainment. *Phys. Fluids* **7** (5), 1095–1106.

KAFTORI, D., HETSRONI, G. & BANERJEE, S. 1995*b* Particle behaviour in the turbulent boundary layer. Part 2. Velocity and distribution profiles. *Phys. Fluids* **7**, 1107.

MARCHIOLI, C. & SOLDATI, A. 2002 Mechanisms for particle transfer and segregation in a turbulent boundary layer. *J. Fluid Mech.* **468**, 283–315.

MATTSON, M. & MAHESH, K. 2011 Simulation of bubble migration in a turbulent boundary layer. *Phys. Fluids* **23**, 045107.

MAXEY, M. R. & RILEY, J. J. 1983 Equation of motion for a small rigid sphere in a non-uniform flow. *Phys. Fluids* **26**, 883.

MESSEGUER, J. 2003 Gene flow assessment in transgenic plants. *Plant Cell, Tissue and Organ Culture* **73** (3), 201–212.

O'CONNELL, L. M., MOSSELER, A. & RAJORA, O. P. 2007 Extensive long-distance pollen dispersal in a fragmented landscape maintains genetic diversity in white spruce. *J. Heredity* **98** (7), 640.

PICANO, F., BATTISTA, F., TROIANI, G. & CASCIOLA, C. M. 2011 Dynamics of PIV seeding particles in turbulent premixed flames. *Exp. Fluids* **50** (1), 75–88.

PICANO, F., SARDINA, G. & CASCIOLA, C. M. 2009 Spatial development of particle-laden turbulent pipe flow. *Phys. Fluids* **21**, 093305.

PICANO, F., SARDINA, G., GUALTIERI, P. & CASCIOLA, C. M. 2010 Anomalous memory effects on transport of inertial particles in turbulent jets. *Phys. Fluids* **22**, 051705.

RIGHETTI, M. & ROMANO, G. P. 2004 Particle–fluid interactions in a plane near-wall turbulent flow. *J. Fluid Mech.* **505**, 93–121.

ROUSON, D. W. I. & EATON, J. K. 2001 On the preferential concentration of solid particles in turbulent channel flow. *J. Fluid Mech.* **428**, 149–169.

SARDINA, G., PICANO, F., SCHLATTER, P., BRANDT, L. & CASCIOLA, C. M. 2011 Large scale accumulation patterns of inertial particles in wall-bounded turbulent flow. *Flow Turbul. Combust.* **86**, 519–532.

SARDINA, G., SCHLATTER, P., BRANDT, L., PICANO, F. & CASCIOLA, C. M. 2012 Wall accumulation and spatial localization in particle-laden wall flows. *J. Fluid Mech.* **699**, 50–78.

SCHLATTER, P. & ÖRLÜ, R. 2010 Assessment of direct numerical simulation data of turbulent boundary layers. *J. Fluid Mech.* **659**, 116–126.

SCHLATTER, P., ÖRLÜ, R., LI, Q., BRETHOUWER, G., FRANSSON, J. H. M., JOHANSSON, A. V., ALFREDSSON, P. H. & HENNINGSON, D. S. 2009 Turbulent boundary layers up to $Re_\theta = 2500$ studied through numerical simulation and experiments. *Phys. Fluids* **21**, 051702.

TOSCHI, F. & BODENSCHATZ, E. 2009 Lagrangian properties of particles in turbulence. *Annu. Rev. Fluid Mech.* **41**, 375–404.